Available online at www.sciencedirect.com
SCIENCE DIRECT®
Journal of Molecular Catalysis A: Chemical 228 (2005) 241–253
JOURNAL OF MOLECULAR CATALYSIS A: CHEMICAL
www.elsevier.com/locate/molcata

An overview of kinetic and spectroscopic investigations on three-way catalysts: mechanistic aspects of the CO + NO and CO + N_2O reactions

P. Granger*, C. Dujardin, J.-F. Paul, G. Leclercq

Université des Sciences et Technologies de Lille, Laboratoire de Catalyse de Lille, UMR CNRS No. 8010, Bâtiment C3, 59655 Villeneuve d'Ascq Cedex, France

Available online 8 December 2004

Abstract

This paper deals with the kinetics of the reduction of nitric oxides by CO, which is a major reaction involved in automotive exhaust three-way catalysts. Spectroscopic and steady state kinetic measurements have been compared in order to explain the different selectivity behavior of Pt- and Rh-based catalysts, particularly during the cold start. It was found that in situ spectroscopy can be a useful tool either for stating on the nature of intermediates or checking the validity of a rate equation. Regarding the kinetics, subsequent calculations and comparisons of thermodynamic and kinetic parameters provide relevant information for modeling purposes. Also, it was found that our kinetic results can be correlated to surface modifications in the particular case of supported bimetallic Pt–Rh catalysts.

Keywords: Kinetics; Three-way catalyst; In situ infrared spectroscopy; N_2O selectivity; CO + NO reaction

1. Introduction

Catalytic reactions promoted over three-way catalysts have been the subject of numerous investigations during the past 30 years, in various ranges of temperature and pressure [1,2]. A particular attention has been paid toward the reduction of NO by CO in N_2, that is a major reaction in automotive exhaust three-way catalysts (TWC). Generally, the reduction of NO by CO is displayed by a two-step reaction involving the intermediate formation of nitrous oxide (N_2O) according to the following sequences:

$$2CO + 2NO \rightarrow N_2 + 2CO_2 \quad (1)$$

$$CO + 2NO \rightarrow N_2O + CO_2 \quad (2)$$

$$CO + N_2O \rightarrow N_2 + CO_2 \quad (3)$$

Typically, TWCs are mainly composed of noble metals (Pt, Rh, and Pd) dispersed on a modified γ-alumina by additives that improve their oxygen storage capacity. Rh is essential for the reduction of NO by CO. Comparative surface science studies under UHV conditions, over single crystals, shown that Rh exhibits the most interesting properties toward the dissociation of NO into chemisorbed N and O atoms with the subsequent desorption of N_2 [3–5]. However, some controversial results are sometimes reported in the literature relative to the observation or not of N_2O. By way of illustration, Castner and Somorjai [6] evidenced significant amounts of N_2O on Rh(s)-[6(1 1 1) × (1 0 0)]. At atmospheric pressure, the formation of N_2O usually occurs whatever the catalyst composition. Nevertheless, Williams and co-workers [7,8] still found from in situ surface Raman spectroscopy on Rh, Pt, and Pd films, that Rh is more selective during the CO + NO reaction. These authors postulated that the higher ability to dissociate, the lower the selectivity for the production of N_2O on Rh. Although, Rh is intrinsically more active, it seems obvious that under typical three-way conditions, the competition between adsorbates may also drastically influence the selectivity [9–12].

Presently, one of the main drawback in the development of three-way catalysts is the incomplete reduction of NO into

* Corresponding author. Tel.: +33 3 20 4938 27; fax: +33 3 20 43 65 61.
E-mail address: pascal.granger@univ-lille1.fr (P. Granger).

1381-1169/$ – see front matter © 2004 Elsevier B.V. All rights reserved.
doi:10.1016/j.molcata.2004.09.081

N_2O, particularly during the cold start engine, N_2O being the main N-containing product in those conditions. Future standard regulations on the emissions of N_2O, and a more stringent legislation on NO_x emissions, should imply further improvements on the catalytic performances of noble metals in order to convert selectively NO into N_2 at lower temperatures and conversions and/or to enhance the subsequent $CO + N_2O$ reaction according to step (3). Up to now, modifications in the composition of three-way catalysts by additives such as ceria, and more recently by ceria–zirconia mixed oxides, sharply enhance their oxygen storage capacity due to the peculiar redox properties of ceria [13–15]. Such modifications significantly promote the activity. Unfortunately, the consequences on the selectivity are not so obvious with sometimes controversial statements regarding the beneficial effect of ceria on the selectivity toward the formation of N_2.

Clearly, subsequent practical improvements on the performances of three-way catalysts, particularly on the selectivity, need probably more details on the composition of the active phases and on the intermediates involved in the formation of N_2O and N_2 during the CO + NO reaction. The clarification of the mechanism schemes either for the formation [16–18], or the subsequent transformation of N_2O, is still questionable [9,10]. By way of illustration, Burch and Coleman [17] recently proposed, from transient kinetic experiments, that the formation of N_2O would mainly proceed via the following step:

$$NO_{ads} + NO_{ads} \rightarrow N_2O + O_{ads}, \quad (4)$$

whereas, previous studies claimed that N_2O mainly forms by reaction between NO_{ads} and N_{ads} [1,2]. Probably, quantitative or semi-quantitative correlations between in situ spectroscopic and kinetic measurements should provide new insights into the functioning mode of three-way catalysts at molecular scale in order to develop more accurate predictive kinetic models. It seems obvious that a better understanding of the role of rhodium, and of the weak effect of Ce addition on the selectivity behavior of TWCs is probably a pre-requisite step for further successful practical developments.

This article reports mechanistic investigations performed in our laboratory in the past decade. Correlations between theoretical calculations, spectroscopic and kinetic measurements allow the selection of a mechanism scheme for the CO + NO and the $CO + N_2O$ reactions. A rate equation has been established which has been checked in a wider range of temperature and conversion above the light-off temperature. Subsequent comparisons of kinetic and thermodynamic parameters for these two reactions obtained on various monometallic and bimetallic noble metal-based catalysts also bring useful arguments for discussing on changes in the selectivity behavior. It was found that correlations between in situ spectroscopic and kinetic measurements can be profitably used either for the identification of intermediate species or for monitoring changes in surface properties of bimetallic Pt–Rh catalysts.

2. Kinetic behavior of supported noble metal based catalysts in the CO + NO reaction—comparisons between Rh, Pt, and Pd

2.1. In situ spectroscopic studies of the CO + NO reaction—correlations with catalytic performances

The development of operando studies, coupling simultaneous in situ spectroscopic and catalytic measurements under transient conditions, can provide relevant information relative to the nature of intermediates involved during catalytic reactions, or of strongly chemisorbed species, which can induce inhibiting effects on the reaction rate [19]. Recently, such an experimental procedure has been successfully operated by Almusaiteer et al. [20] and Chafik et al. [18], respectively, on Pd and Rh. These authors observed the development of positively, neutral, and negatively charged NO species either on Rh or Pd during the CO + NO reaction. The formation of gem-dinitrosyl NO species has also been earlier mentioned on Rh [21]. Changes in the strength of the metal–NO bond is usually assigned to the electron-withdrawing effect of oxygen atoms, from the dissociation of NO, which accumulate on the surface, further lowering the extent of electron-backdonation into the molecular anti-bonding orbital π^* of NO [21]. Hence, it is generally accepted that the N–O bond breaking is easier in the case of bent $Rh–NO^-$ species. Both studies agree with the formation of N_2O on oxidic palladium and rhodium species. However, some divergences arise with regard to the nature of intermediates involved in the formation of N_2O. Almusaiteer et al. propose that N_2O comes from nitrosyl species, whereas Chafik et al. suggest the involvement of dinitrosyl species $Rh(NO)_2$. Nevertheless, these latter authors do not completely exclude nitrosyl species $Rh–NO^+$ as possible intermediate according to Liang et al. [21] who suggested the existence of some degree of reversibility between $Rh(NO)_2$ and $Rh–NO^+$ according to the following reaction:

$$Rh–NO^+ + NO_g \Leftrightarrow Rh(NO)_2 \quad (5)$$

An alternative route involving isocyanate species stabilised over W^{6+}-doped Rh/TiO_2 catalysts has been proposed [16]. Such a suggestion seems more controversial with previous investigations which report from pulse transient IR studies on Rh/SiO_2, that NCO is not directly involved in the formation of CO_2 but more probably acts as spectator [22,23]. In the light of these above-mentioned observations, different elementary steps have been suggested in the literature for explaining the formation of N_2O:

$$Rh^0–NO^- + Rh^0–N \rightarrow 2Rh^0 + N_2O \quad (6)$$

$$Rh(NO)_2 + Rh–N + NO \rightarrow Rh–NO^+ + Rh^0–NO^- + N_2O \quad (7)$$

$$Rh–NCO + NO \rightarrow Rh + N_2O + CO \quad (8)$$

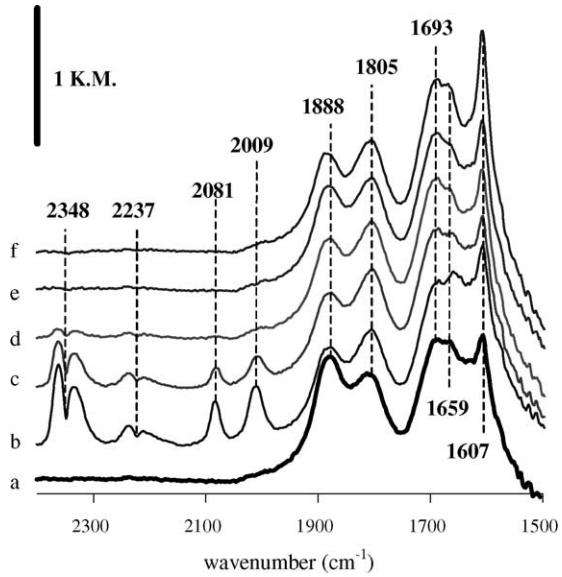

Fig. 1. IR spectra during CO pulses under a continuous 1% NO/He flow on Rh/Al_2O_3 at 300 °C: before CO pulses (a); beginning of the first CO pulse (b); middle of the first CO pulse (c); end (d); after the first pulse (e); flush under helium after eight CO pulses (f) [24].

2.1.1. *Operando infrared spectroscopic studies on Rh/Al_2O_3*

Recent operando spectroscopic measurements, performed in our laboratory on Rh/Al_2O_3 during the CO + NO reaction, show that positively ($Rh–NO^+$), neutral (Rh–NO) and negatively charged NO species, respectively, at 1888, 1805, and 1693 cm^{-1} predominate on Rh [24–26] (see Fig. 1a). Fig. 2 illustrates the sequence when a pre-adsorbed NO surface is exposed to successive CO pulses at 300 °C. Clearly, the disappearance of the $Rh–NO^+$ band (1869 cm^{-1}) is in connection with the development of the typical 2243 cm^{-1} band assigned to gaseous N_2O. The sudden overestimation, of the relative mass spectrometer signal of CO_2^+ ($m/e = 44$) primary ionisation compared to the CO_2^{2+} double ionisation ($m/e = 22$) emphasizes an extra formation of N_2O that is not observed when a pre-adsorbed CO surface is exposed to successive NO pulses (see Fig. 3). During this sequence, mainly neutral NO species have been observed (1810 cm^{-1}) [24]. Further transient experiments when CO and NO co-adsorb and react at 300 °C (Fig. 1) highlight a similar correlation between the formation of N_2O on Rh/Al_2O_3 and a more extensive attenuation of the IR band assigned to $Rh–NO^+$ species, that could act as intermediate in the production of N_2O, while neutral NO species would be mainly involved in the formation of N_2.

2.1.2. *In situ surface Raman spectroscopy on Pd/Al_2O_3*

Similar trends were observed from in situ Raman spectroscopic measurements during temperature programmed CO + NO reaction on bulk and supported Pd catalysts [27,28]. Resonance Raman effects can be profitably used for characterising the formation of palladium oxide [29,30]. As exemplified in Fig. 4, the formation of PdO, characterised by Raman lines at 640 and 420 cm^{-1}, corresponding to the Raman B_{1g} and E_g vibrational modes of PdO, develops mainly on 1 wt.% Pd/Al_2O_3 during time on stream, while bulk Pd preserves its metallic character (see Fig. 5). Additional spectral features at low wavenumbers are observable associated to vibrational stretching modes of chemisorbed N, NO and CO species coordinated to Pd^0 [7,8,27,28]. These observations shown that this technique is an interesting in situ time probe for investigating catalytic mechanisms. Raman features in Fig. 5 are in qualitative agreement with previous assignments, the vibrational stretching mode of Pd–N of chemisorbed N atoms and NO molecules are distinguishable, respectively, at 277 and 314 cm^{-1}. An additional line at 356 cm^{-1} characterised adsorbed CO molecules. Contrarily to bulk Pd, chemisorbed NO species on 1 wt.% Pd/Al_2O_3 stabilise at 300 °C which has been related to the development of less reactive $Pd–NO^{\delta+}$ species towards the dissociation, as exemplified in Fig. 6. Such differences in spectral features

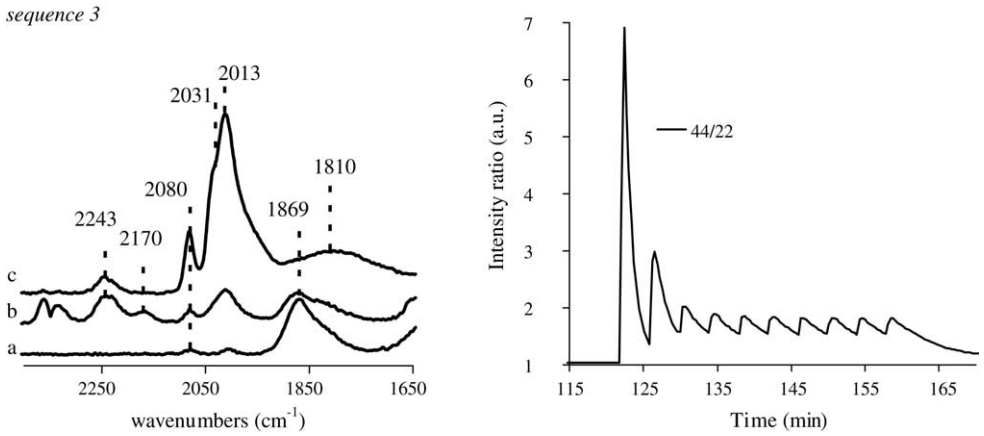

Fig. 2. IR spectra and MS analyses obtained on pre-adsorbed NO on Rh/Al_2O_3 after successive CO pulses at 300 °C: before CO pulses (a); during the first CO pulse (b); during the second CO pulse (c) [24].

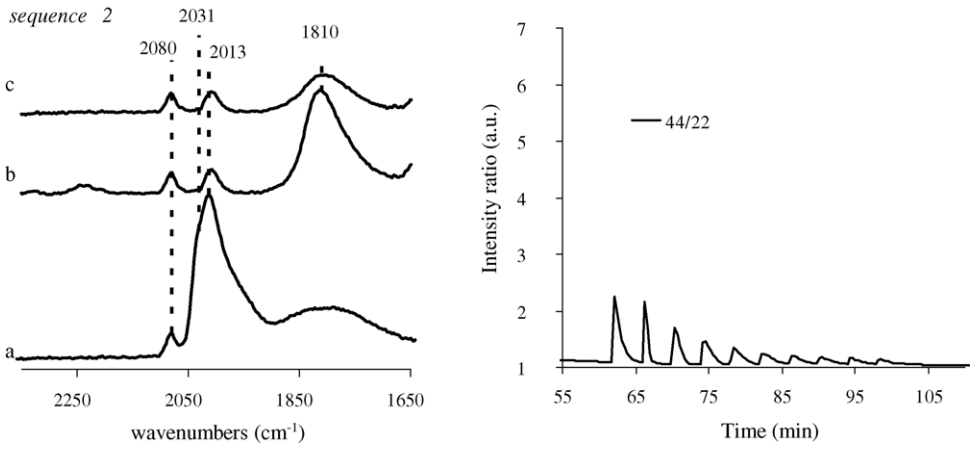

Fig. 3. IR spectra and MS analyses obtained on pre-adsorbed CO on Rh/Al_2O_3 after successive NO pulses at 300 °C: before NO pulses (a); during the first NO pulse (b); during the second NO pulse (c) [24].

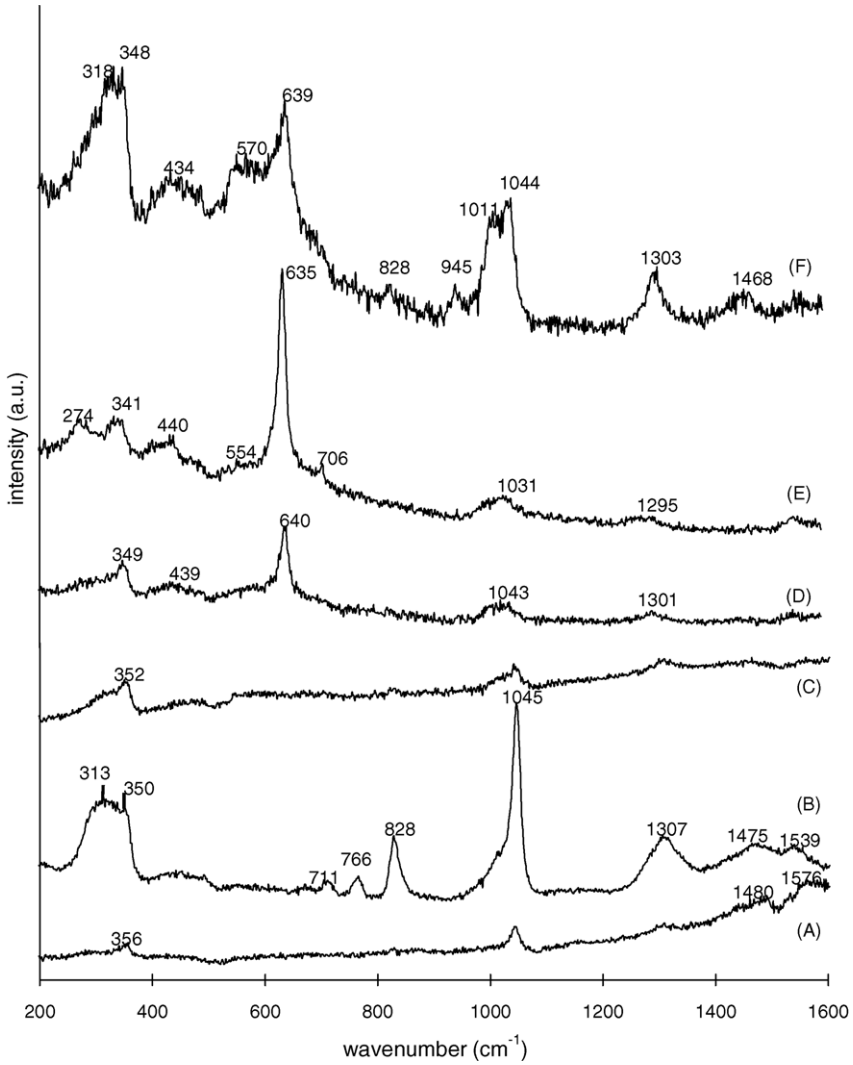

Fig. 4. In situ Raman spectra obtained on a pre-reduced 1 wt.% Pd/Al_2O_3 catalyst during the CO + NO reaction in stoichiometric conditions with 5×10^{-3} atm NO and 5×10^{-3} atm CO at: (A) 25 °C; (B) 50 °C; (C) 100 °C; (D) 200 °C; (E) 300 °C; (F) after cooling at 25 °C—(spectrum (F) was multiplied by 0.5) [23].

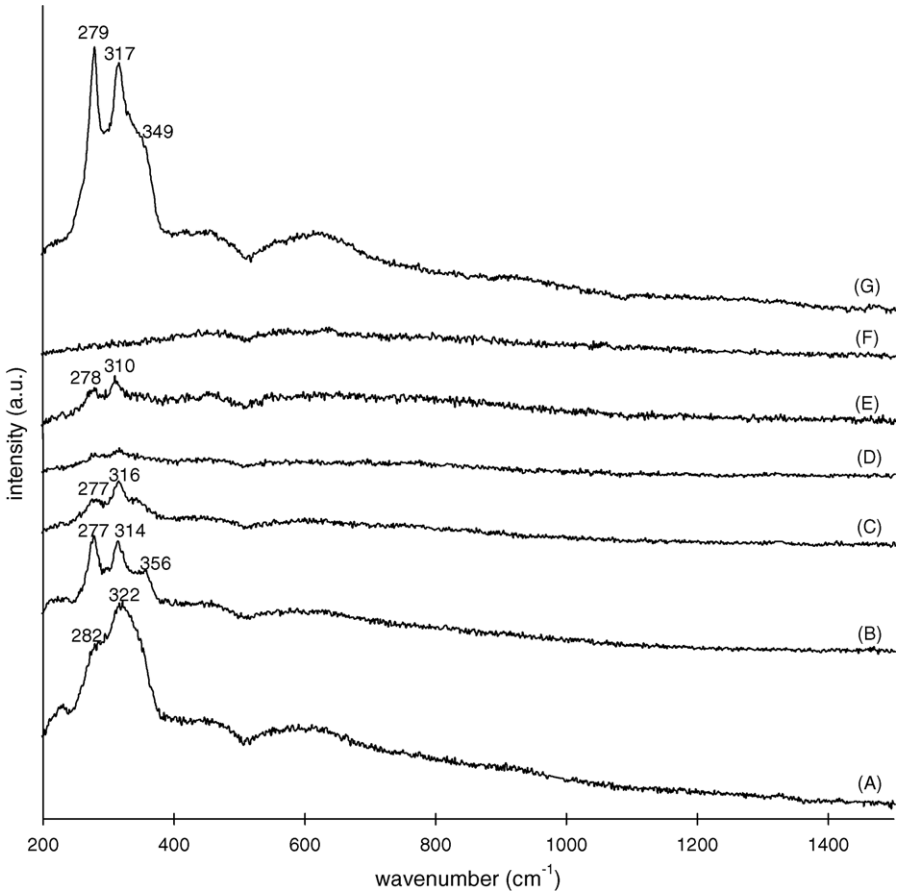

Fig. 5. In situ Raman spectra obtained on a pre-reduced bulk Pd catalyst during the CO + NO reaction in stoichiometric conditions with 5×10^{-3} atm NO and 5×10^{-3} atm CO at: (A) 25 °C; (B) after 1 h exposure at 25 °C; (C) 50 °C; (D) 100 °C; (E) 200 °C; (F) 300 °C; (G) after cooling at 25 °C—(spectrum (G) was multiplied by 0.5) [23].

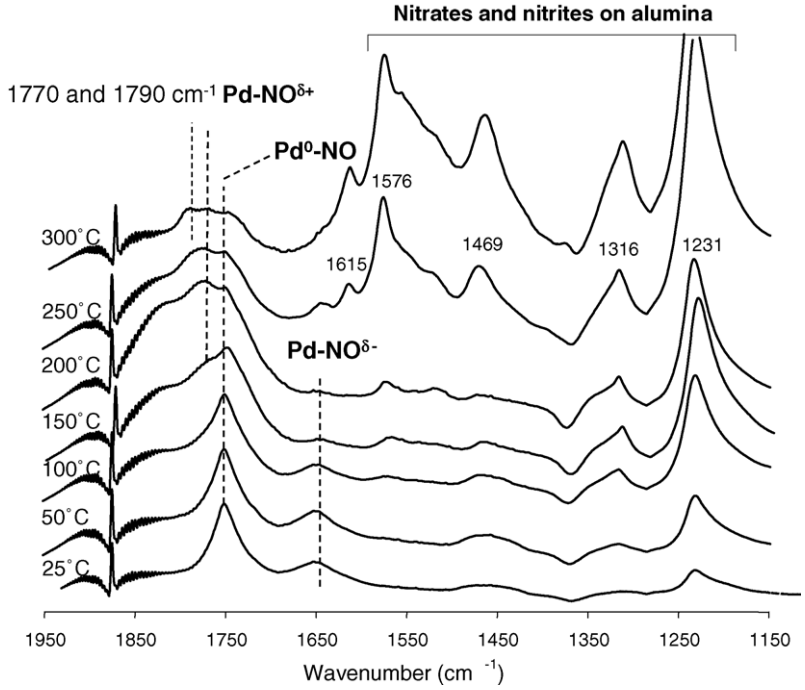

Fig. 6. In situ infrared spectra in the course of the CO + NO reaction on a pre-reduced 1 wt.% Pd/Al_2O_3 in stoichiometric conditions with 5×10^{-3} atm NO and 5×10^{-3} atm CO.

Table 1
Steady-state catalytic performances of Pd-based catalysts in the CO + NO reaction at 300 °C [25]

Catalysts	Metal dispersion (%)	Intrinsic rate (molecules h^{-1} surface at^{-1})	N_2O selectivity
Bulk Pd	1.4	12	0.32
1 wt.% Pd/Al_2O_3	40	373	0.62

correspond to significant changes in the catalytic behavior of supported and bulk Pd catalysts. As indicated in Table 1, the formation of N_2O is more accentuated on 1 wt.% Pd/Al_2O_3 than on bulk Pd. Such a difference has been associated to the segregation of smaller Pd particles on alumina much more oxidisable than those in the bulk catalyst [27].

Finally, both observations on Rh/Al_2O_3 and Pd/Al_2O_3 are in agreement with previous IR observations relative the involvement of oxidic Pd and Rh species in the formation of N_2O. On the other hand, our conclusions slightly differ from those earlier suggested as far as concerned the nature of intermediates in the formation of N_2O. Correlations between spectroscopic and catalytic measurements show that N_2O could originate from $Rh–NO^+$, while neutral and/or negatively charged NO species, that dissociate more easily, would lead more probably to the production of nitrogen. It was also found that the accumulation of strongly adsorbed O and/or NO species mainly on 1 wt.% Pd/Al_2O_3, contrarily to bulk Pd, have some repercussions on the subsequent $CO + N_2O$ reaction. These strongly adsorbed species probably prevent the re-adsorption of N_2O and its further decomposition into N_2 in the course of the CO + NO reaction [23].

2.2. Kinetics of the CO + NO reaction on monometallic Rh, Pt and Pd catalysts

Various mechanism proposals listed in the literature mainly differ from the step of NO transformation [31–36]. Previous investigations suggested a bimolecular reaction between NO_{ads} and CO_{ads} on Pd [33]. Alternately, the dissociation of gem-dinitrosyl [17,34] or nitrosyl species [35–37] has been proposed. Moreover, the involvement of gem-dinitrosyl species as possible intermediate in the formation of N_2 and N_2O is supported by earlier theoretical calculations using extended Huckel methods [38] which shown that the formation of NO dimer species $(NO)_2$ likely occurs on Rh(1 0 0). A strengthening of the N–N parallel to a weakening of the terminal N–O bond more accentuated than in monomer NO species is consistent with an easier N–O bond breaking. Hence, the better selectivity of Rh-based catalysts could be explained by the involvement of dinitrosyl species. In that case, the production of N_2 would preferentially occur via the following step: $2NO_{ads} \rightarrow N_2 + 2O_{ads}$. As a matter of fact, steady-state rate measurements performed on Pt/Al_2O_3 [36] and Rh/Al_2O_3 [39] disagree with this proposal for explaining the formation of N_2 and N_2O. It has been found that the more representative mechanism involves the following sequences:

$$NO + * \Leftrightarrow NO_{ads} \quad (9)$$

$$NO + * \Leftrightarrow NO_{ads} \quad (10)$$

$$NO_{ads} + * \rightarrow N_{ads} + O_{ads} \quad (11)$$

$$NO_{ads} + N_{ads} \rightarrow N_2 + O_{ads} + * \quad (12)$$

$$NO_{ads} + N_{ads} \rightarrow N_2O + 2* \quad (13)$$

$$N_{ads} + N_{ads} \rightarrow N_2 + 2* \quad (14)$$

$$CO_{ads} + O_{ads} \rightarrow CO_2 + 2* \quad (15)$$

A rate expression can be derived that correctly fits the partial dependency of the rate at 300 °C by assuming that the adsorption of the reactants takes place in equilibrium, with the surface mainly covered by chemisorbed CO and NO molecules. Generally speaking, the key step is the dissociation of NO_{ads} usually considered as rate determining.

$$r_{NO} = \frac{k\lambda_{NO}P_{NO}}{(1 + \lambda_{NO}P_{NO} + \lambda_{CO}P_{CO})^2}, \quad (16)$$

where k is the rate constant related to the step of NO dissociation, λ_i and P_i being, respectively, the equilibrium adsorption constant and the partial pressure of the compound i (with i = NO or CO).

The adjusted values for k and λ_i in Table 2 emphasise the fact that NO adsorbs more strongly and dissociates more readily on Rh than on Pt and 10 wt.% Pd/Al_2O_3 by comparing the value of the intrinsic rate constant k and λ_{NO}. On the other hand, no clear correlation was obtained on 1 wt.% Pd/Al_2O_3 using Eq. (16). In accordance with previous spectroscopic observations the oxygen coverage cannot be neglected on 1 wt.% Pd/Al_2O_3 at 300 °C. Such an accumulation of chemisorbed O atoms could also underline a shift of the rate limiting from step (12) to step (15) in accordance with earlier investigations [40]. Consequently, both observations probably invalidate Eq. (16) on 1 wt.% Pd/Al_2O_3.

Now, regarding elementary steps (12)–(14) related to the formation of N_2 and N_2O, the NO partial pressure dependency of the selectivity toward the formation of N_2O (S_{N_2O}) on Pt/Al_2O_3 depends on the relative ratio [36]:

$$\frac{r_{N_2}}{r_{N_2O}} = \frac{k_{12}}{k_{13}} + 2\left[1 + \frac{k_{12}}{k_{13}}\right]\frac{k_{14}k_{11}}{(k_{12} + k_{13})^2\lambda_{NO}P_{NO}} \quad (17)$$

The selectivity behavior of Rh/Al_2O_3 differs from that of Pt/Al_2O_3 mainly by the weak sensitivity of $S_{N_2O}$to the reaction conditions (temperature, pressure conditions) [39,41]. Such a weak dependence earlier observed on Rh could reflect the involvement of a common reaction path for the formation

Table 2
Comparison of kinetic and thermodynamic parameters calculated at 300 °C for the CO + NO reaction on various supported noble metal-based catalysts

Catalysts	k[a]	k'[b]	λ_{NO} (atm^{-1})	λ_{CO} (atm^{-1})	Reference
1 wt.% Pt/Al_2O_3	11.4×10^{-3}	404	11	121	[36]
0.2 wt.% Rh/Al_2O_3	225×10^{-3}	12315	412	71	[39]
10 wt.% Pd/Al_2O_3	830×10^{-3}	3585	373	236	

[a] Specific rate constant (mol h^{-1} g^{-1}).
[b] Intrinsic rate constant (molecules h^{-1} at_s^{-1}).

of N_2O and N_2 [41]. On the basis of Eq. (17), it could be explained by much higher values for the rate constants k_{12} and k_{13} compared to k_{14} or k_{11}, or a much higher value for λ_{NO} on Rh/Al_2O_3. In any case, the surface of Rh would be predominantly covered by NO compared to Pt. Consequently, steps (12) and (13) are likely much faster on Rh/Al_2O_3 than step (14). Hence, Eq. (18) correctly represents the selectivity on Rh/Al_2O_3 [39].

$$\frac{r_{N_2}}{r_{N_2O}} \cong \frac{k_{12}}{k_{13}} \tag{18}$$

Both kinetic data emphasise previous statements from spectroscopic observations relative to the involvement of nitrosyl species as intermediates in the formation of N_2O and N_2. Accordingly, nitrosyl species involved in steps (12) and (13) could differ from the strength of the metal–NO bond and their ability to dissociate.

3. Kinetics of the CO + NO reaction on bimetallic Pt–Rh catalysts

3.1. On a freshly prepared $Pt–Rh/Al_2O_3$

In the case of the kinetic behavior of bimetallic $Pt–Rh/Al_2O_3$, two borderline cases can be considered. Competitive adsorptions of the reactants can be assumed if the interaction between the two metals averaged the electronic properties of rhodium and platinum. Alternately, both metals can preserve their peculiar adsorption properties in accordance with previous observations of Ng et al. [42] who found on $Pt_{10}Rh_{90}$ (1 1 1) that Pt, much less active than Rh, acts as a dilutant further lowering the overall activity in the CO + NO reaction. Nevertheless, these authors do not rule out possible electronic modifications. The fact that supported Pt and Rh catalysts could retain their individual adsorption properties is also supported by Van Slooten and Nieuwenhuys [43] who investigated the co-adsorption of CO and NO on $Pt–Rh/SiO_2$. These authors observed preferential adsorptions of NO on Rh and CO on Pt. In our case, further comparisons of the equilibrium adsorption constants of NO and CO on Pt/Al_2O_3 and Rh/Al_2O_3 in Table 2 speak in favor of preferential adsorptions of NO on Rh and CO on Pt. Based on this hypothesis, the composition of the nearest-neighbor vacant site is questionable since it could be only composed of Rh, Pt, or either Pt or Rh. In fact, the best fit between experimental and predicted rates is obtained with the following equation, which accounts for a vacant site mainly composed of Pt [39].

$$r_{NO} = k\theta_{NO}(1 - \theta_{CO}) = \frac{k\lambda_{NO}P_{NO}}{(1 + \lambda_{NO}P_{NO})(1 + \lambda_{CO}P_{CO})}, \tag{19}$$

Further, in situ transmission infrared spectroscopic investigation of the CO + NO reaction on $Pt–Rh/Al_2O_3$ agree with preferential adsorptions of NO on Rh and CO on Pt in the case of $Pt–Rh/Al_2O_3$. As illustrated in Fig. 7, the infrared band at 2071 cm^{-1} mainly characterises linear CO species on Pt^0 sites, while the 1708, 1825 at 1900 cm^{-1} bands correspond to the usual vibrational modes of nitrosyl species coordinated on Rh [21,26]. No IR band relative to NO and CO chemisorbed, respectively, on Pt and Rh are discernible.

Eq. (19) has been checked in a wider range of temperature and conversion. Temperature-programmed NO conversion curves obtained in differential conditions can be correctly modelled using Eq. (20) that accounts for the partial pressure dependencies (i.e. the surface coverage) of the adsorption enthalpies of NO and CO according to Freundlich's

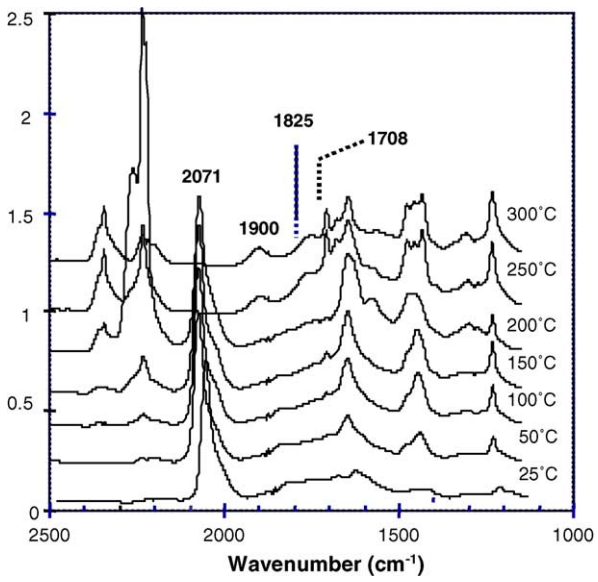

Fig. 7. In situ IR spectra recorded on a pre-reduced $Pt–Rh/Al_2O_3$ catalyst in the course of the CO + NO reaction with 5×10^{-3} atm NO and 5×10^{-3} atm CO.

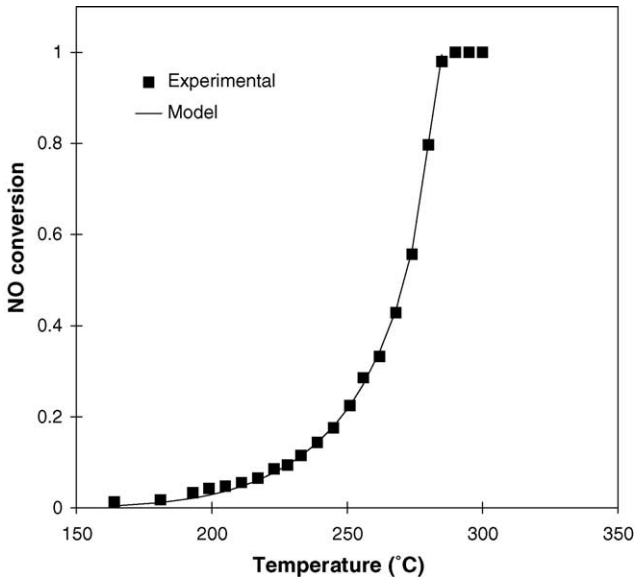

Fig. 8. Comparison between experimental and predicted conversions on Pt–Rh/Al_2O_3 in stoichiometric conditions with 5×10^{-3} atm NO and 5×10^{-3} atm CO [44].

assumptions [44].

3.2. Effects of deactivation on the kinetic behaviour of Pt–Rh/Al_2O_3

Catalyst deactivation may drastically affect the reaction rate since it can be caused by—a decrease in the number of active sites—a modification in the quality of the active site. Under three-way conditions, alloying effects can be significant and drastically altered the catalytic performances of bimetallic Pt–Rh catalysts [48]. These effects can be mimicked by submitting Pt–Rh/Al_2O_3 to a thermal sintering under wet atmosphere at 800 °C [49]. A loss of metal dispersion from 0.64 to 0.27 and a surface Rh enrichment occur during thermal sintering. Eq. (19) based on non-competitive adsorptions is invalidated on the sintered Pt–Rh/Al_2O_3 catalyst [47]. As a matter of fact, it mimics the behavior of a mono-metallic catalysts with competitive adsorptions of the reactants. The calculations of the rate constant k and λ_i using Eq. (16) lead to comparable values obtained on Rh/Al_2O_3 according to the margin of error (see Table 3). Such comparisons agree with a surface Rh enrichment in accordance with previous infrared spectroscopy of CO adsorbed [49].

Various comments arise from these comparisons. Clearly, spectroscopic measurements help to check a posteriori the assumptions for establishing a rate equation. In addition kinetics could be a useful tool for characterising surface compositions and subsequent changes induced in the course of the reaction compared to classical physico-chemical techniques, such as X-ray photoelectron spectroscopy involving a ultra-high vacuum.

$$r_{NO} = \frac{1.74 \times 10^8 \exp[(-13697 - 492 \ln P_{NO} - 186 \ln P_{CO})/T](1-\tau_{NO})P^0_{NO}}{(1 + 2.9 \times 10^{-2} \exp[(793 - 492 \ln P_{NO} - 186 \ln P_{CO})/T](1-\tau_{NO})P^0_{NO})(1 + 2.1 \times 10^{-1} \exp[(474 - 156 \ln P_{NO} - 112 \ln P_{CO})/T](1-\tau_{CO})P^0_{CO})} \quad (20)$$

with

$$\tau_{CO} = \tau_{NO}\left[\frac{1.33 + \tau_{NO}(2.2 \times 10^{-7} \exp \lfloor 6330/T \rfloor - 1.33)}{2 + \tau_{NO}(2.2 \times 10^{-7} \exp[6330/T] - 2)}\right] \quad (21)$$

By way of illustration, the correlation between experimental and predicted conversion curves, in Fig. 8 on Pt–Rh/Al_2O_3 shows a good fit.

As shown in Table 3, the adjusted values for λ_{CO} and λ_{NO} on Pt–Rh/Al_2O_3, close to those obtained, respectively, on Pt/Al_2O_3 and Rh/Al_2O_3, emphasise the occurrence of preferential adsorption of NO on Rh and of CO on Pt. The very low value obtained for k on Pt–Rh/Al_2O_3 compared to that obtained on Rh could reflect a surface Pt enriched catalyst with a random distribution of Rh atoms at the surface. Alternately, it could be in connection with different locations of Pt and Rh atoms in the bimetallic particles since it is generally accepted that the dissociation of NO is structure sensitive [45–47].

3.3. Influence of Ce addition on the kinetic behaviour of Pt–Rh/Al_2O_3

As illustrated in Fig. 9, the conversion profile on Pt–Rh/Al_2O_3–CeO_2 usually tends towards lower tempera-

Table 3
Comparison of kinetic and thermodynamic parameters calculated at 300 °C for the CO + NO reaction on supported bimetallic Pt–Rh on alumina

Catalysts	k[a]	k'[b]	λ_{NO} (atm^{-1})	λ_{CO} (atm^{-1})	Reference
1 wt.% Pt–0.2 wt.% Rh/Al_2O_3	4.74×10^{-3}	469	505	122	[39]
Sintered Pt–Rh/Al_2O_3	11.9×10^{-3}	623	448	85	[49]

[a] Specific rate constant (mol h^{-1} g^{-1}).
[b] Intrinsic rate constant (molecules h^{-1} at_s^{-1}).

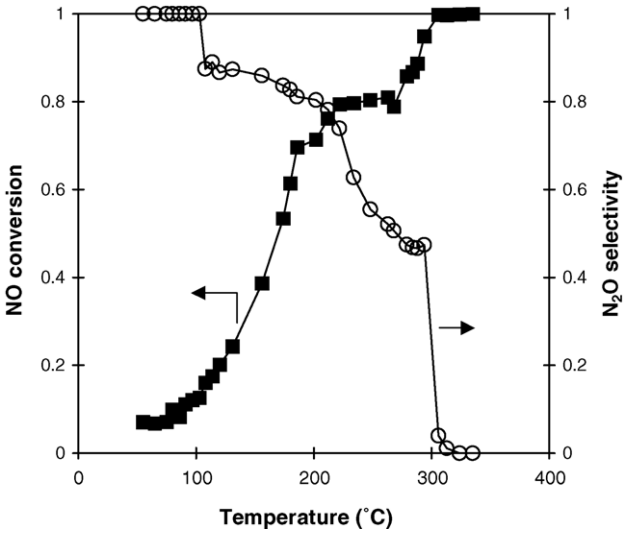

Fig. 9. Temperature-programmed conversion and selectivity curves on Pt–Rh/Al_2O_3–CeO_2 in the course of the CO + NO reaction with 5×10^{-3} atm NO and 5×10^{-3} atm CO.

tures. This synergy effect on the activity due to interactions between noble metals and ceria strongly attenuates with a rise in temperature. Above 280 °C, Pt–Rh/Al_2O_3–CeO_2 and Pt–Rh/Al_2O_3 behave similarly [50–52]. It was also found that no significant enhancement on the initial selectivity and on the subsequent reduction of N_2O is obtained after ceria addition.

The beneficial effect of ceria on the kinetic behavior of noble metals can be explained either by a mono- or a bi-functional mechanism involving the reactivity of oxygen from ceria at the vicinity of metallic particles. The subsequent formation of anionic vacancies can provide active sites that can potentially dissociate NO. Consequently, the rate enhancement can be explained by the following sequences:

$$CO + * \Leftrightarrow CO_{ads} \quad (9)$$

$$NO + * \Leftrightarrow NO_{ads} \quad (10)$$

$$CO_{ads} + \text{“O”} \rightarrow CO_{2g} + \text{“V”} + * \quad (22)$$

$$NO_{ads} + \text{“V”} \rightarrow N_{ads} + \text{“O”} + * \quad (23)$$

$$NO_{ads} + N_{ads} \rightarrow N_2 + O_{ads} + * \quad (12)$$

$$NO_{ads} + N_{ads} \rightarrow N_2O + 2* \quad (13)$$

$$N_{ads} + N_{ads} \rightarrow N_2 + 2* \quad (14)$$

where “V” and “O” stand for anionic vacancies and reactive oxygen species on ceria, respectively.

Alternately, only noble metals could catalyse the CO + NO reaction on Pt–Rh/Al_2O_3–CeO_2. In such a case, ceria would mainly influence the adsorption properties of noble metals with subsequent modifications of the relative rates of steps (9)–(15). Such an explanation is in line with previous findings made by Oh [53] who found that ceria strongly favors the adsorption and the dissociation of NO on Rh. Consequently, kinetic data on ceria modified TWCs could be predicted using a kinetic model that derives either from a mono-functional mechanism, involving only noble metals, or a bi-functional mechanism including steps on ceria [54,55]. Accordingly, the following Eq. (24) that accounts for the mono- and bi-functional mechanism can be considered for modelling the conversion in the whole range of TP conversion curves.

$$r_{NO} = r_1 + r_2 \quad (24)$$

$$r_{NO} = \frac{k\lambda_{NO}P_{NO}}{(1+\lambda_{CO}P_{CO})(1+\lambda_{NO}P_{NO})} + \frac{k_{22}k_{23}\lambda_{NO}\lambda_{CO}P_{NO}P_{CO}}{k_{23}\lambda_{NO}P_{NO}(1+\lambda_{CO}P_{CO}) + k_{22}\lambda_{CO}P_{CO}(1+\lambda_{NO}P_{NO})}$$

Comparisons of the optimized rate constants k, k_{22}, k_{23}, in Table 4, from kinetic measurements performed at 120 °C show that steps on ceria prevail, the bi-functional mechanism being the most likely on Pt–Rh/Al_2O_3–CeO_2 at 120 °C. Consequently, at low temperature Eq. (24) can be simplified $r_{NO} \cong r_2$.

The relative rate constant k_{22}/k_{23} ~1400 at 300 °C suggests an extensive surface reduction of ceria, with a very low surface concentration of reactive oxygen species available, that indicates a reaction mainly catalyses by noble metals. In that case, the mono-functional mechanism prevails ($r_{NO} \cong r_1$). Further comparisons of the equilibrium constants of NO and CO at 300 °C in Table 4 also indicate that the interaction between reduced ceria and noble metal particles modifies their adsorption properties with a weakening of the adsorption of the reactants [51].

Table 4
Influence of ceria on the kinetic behavior of noble metals

Catalysts	T (°C)	k[a]	k_{32}[a]	k_{33}[a]	λ_{NO} (atm^{-1})	λ_{CO} (atm^{-1})	Reference
Pt–Rh/Al_2O_3	300	4.74×10^{-3}	–	–	505	122	[39]
Pt–Rh/Al_2O_3–CeO_2	300	38.5×10^{-3}			12.1	29.9	[51]
	120	2.7×10^{-4}	89.5×10^{-3}	1.2×10^{-3}	353	751	[51]

[a] Specific rate constant (mol h^{-1} g^{-1}).

4. Mechanism of the single CO + N_2O reaction on supported monometallic and bimetallic Pt–Rh on Al_2O_3

Presently, there is no consensus on the mechanism of the CO + N_2O reaction. Most of them differ from the step of N_2O transformation. A dissociative N_2O adsorption is proposed under ultra high vacuum between 427 and 1327 °C [56]. On the other hand, the decomposition of N_2O at higher pressure on Pt [57], or its reduction in the presence of CO on Rh/Al_2O_3 [6] has been depicted by a mechanism involving a molecular N_2O adsorption prior to dissociation. A two-step mechanism involving the intermediate formation chemisorbed N_2O molecules (N_2O_{ads}) has also been considered on rhodium-based catalysts [58–62]. In that case, the involvement of a nearest-neighbor vacant site is questionable because of the steric hindrance of N_2O_{ads}. Indeed, previous studies shown that the adsorption and the subsequent dissociation of N_2O need geometrical requirements [63]. In fact, the orientation N_2O molecules adsorbed via the terminal N or O atom may drastically influence on the elementary steps [63–65], with a dissociation involving or not an additional site. Steady state kinetic measurements on Pt/Al_2O_3 [62], Rh/Al_2O_3, and $Pt–Rh/Al_2O_3$ [12] at 300 °C agree with the following mechanism scheme where N_2O dissociates on a nearest-neighbor vacant site.

$$CO + * \Leftrightarrow CO_{ads} \quad (9)$$

$$N_2O + * \Leftrightarrow N_2O_{ads} \quad (25)$$

$$N_2O_{ads} + * \rightarrow N_2 + * + O_{ads} \quad (26)$$

$$N_2O_{ads} + * \rightarrow N_{2,ads} + O_{ads}$$

$$CO_{ads} + O_{ads} \rightarrow CO_2 + 2* \quad (15)$$

A rate equation can be established from a similar set of assumptions earlier mentioned for the CO + NO reaction.

$$r_{N_2O} = \frac{k_{26}\lambda_{N_2O}P_{N_2O}}{(1 + \lambda_{CO}P_{CO} + \lambda_{N_2O}P_{N_2O})^2} \quad (27)$$

Further theoretical calculations based on the Density Functional Theory summarised in Table 5 and Fig. 10 show that the adsorption of N_2O on Pt and Rh clusters composed of four atoms, mainly occurs via the terminal N atoms and induces a lengthening of the N–N and the terminal N–O bond. The stabilisation of bent N_2O molecules linked to two adjacent Rh atoms leads to a more extensive weakening of the terminal N–O bond than on Pt. Such a comparison is in agreement with changes of the intrinsic rate constant of N_2O dissociation on Rh/Al_2O_3 and Pt/Al_2O_3, of respectively 3400 and 1000 molecules h^{-1} at_s^{-1}, which indicate a better N_2O dissociation on Rh.

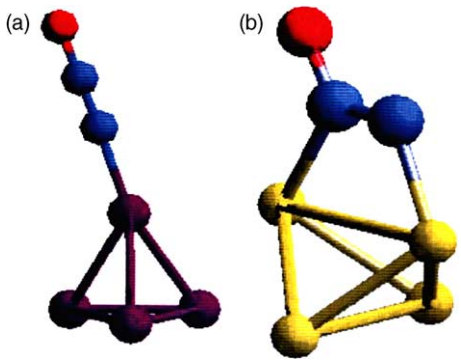

Fig. 10. Optimised geometrical configurations of chemisorbed N_2O molecules on noble metal clusters (composed of four atoms) using DFT calculations: (a) Pt_i (b) Rh.

Subsequent modifications by Ce addition lead to a significant enhancement of the overall activity during the single reduction of N_2O by CO reflected by a significant shift of the light-off temperature toward lower values. It is worthwhile to note that the synergy effect on the activity is preserved on the whole range of conversion of temperature-programmed experiments (see Fig. 11) contrarily to previous observations

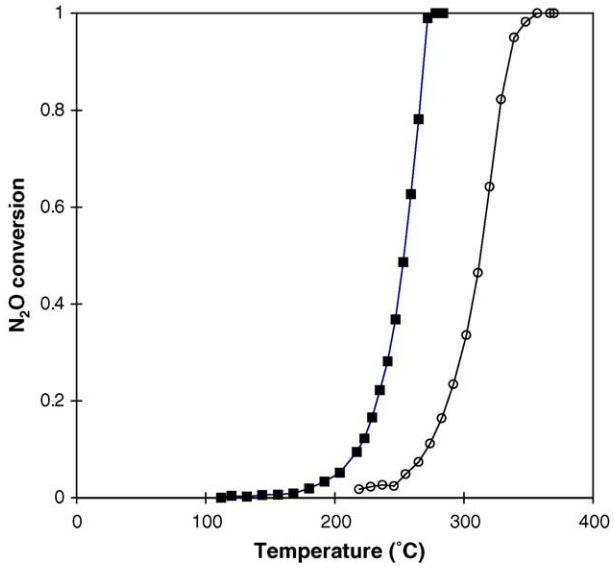

Fig. 11. Temperature-programmed CO + N_2O reaction on $Pt–Rh/Al_2O_3$ (◯) and $Pt–Rh/Al_2O_3–CeO_2$ (■) in stoichiometric conditions with 5×10^{-3} atm CO and 5×10^{-3} atm N_2O.

Table 5
Geometrical features of chemisorbed N_2O molecule on Pt- and Rh-based clusters

Cluster	Distance M—N (Å)	Distance N—N (Å)	Distance N—O (Å)	Angle NNO (°)
Pt	1.96	1.14	1.19	180
Rh	1.87	1.25	1.24	128

for the CO + NO reaction. Similarly, such a synergy effect can be correctly explained by the following steps involving ceria:

$$CO_{ads} + \text{“O”} \rightarrow CO_{2g} + \text{“V”} + * \quad (22)$$

$$N_2O_{ads} + \text{“V”} \rightarrow N_{2,ads} + \text{“O”} \quad (28)$$

$$N_2O_{ads} + \text{“V”} \rightarrow N_2 + \text{“O”} + *$$

then Eq. (29) can be established accounting for the mono-functional mechanism, restricted to noble metals, and the bi-functional one involving the redox properties of ceria [66].

$$r_{N_2O} = \frac{k_{26}\lambda_{N_2O}P_{N_2O}}{(1+\lambda_{CO}P_{CO}+\lambda_{N_2O}P_{N_2O})^2} + \frac{k_{22}k_{28}\lambda_{N_2O}\lambda_{CO}P_{N_2O}P_{CO}}{k_{28}\lambda_{N_2O}P_{N_2O}(1+\lambda_{CO}P_{CO}) + k_{22}\lambda_{CO}P_{CO}(1+\lambda_{N_2O}P_{N_2O})} \quad (29)$$

It was found that the bi-functional mechanism prevails in the whole range of conversion. TP conversion profiles can be correctly predicted after simplification of Eq. (29) by neglecting the term relative to the mono-functional mechanism. At 300 °C, the relative rate k_{22}/k_{28} of 0.34 clearly indicates that oxygen species from ceria predominate at the surface contrarily to previous observations during the CO + NO reaction. Consequently, the synergy effect on the reduction of N_2O by CO is preserved on Pt–Rh/Al_2O_3–CeO_2.

5. Which parameters govern the selectivity for the production of N_2O?

In a first approach, it could be postulated that the higher the ability to dissociate N_2O on Rh, the lower the selectivity towards N_2O formation during the CO + NO reaction on that noble metal. In fact, the selectivity curves in Fig. 12 cannot be completely explained based on the intrinsic properties of Rh toward the dissociation of N_2O. Consistently, the selectivity mainly depends on the competition between adsorbates. Table 6 shows significant changes in the equilibrium constants of N_2O and NO suggesting that the competition between NO and N_2O probably governs the selectivity behavior of Pt and Rh. Their comparisons show that the adsorption of N_2O is favored on Pt, which can re-adsorb and react more readily than NO_{ads} species on Pt. Such a statement correctly explains the continuous decrease in the selectivity of Pt/Al_2O_3 with a rise in conversion. On the other hand, the stronger NO adsorption on Rh/Al_2O_3 and Pt–Rh/Al_2O_3 prevents the re-adsorption of N_2O and its subsequent

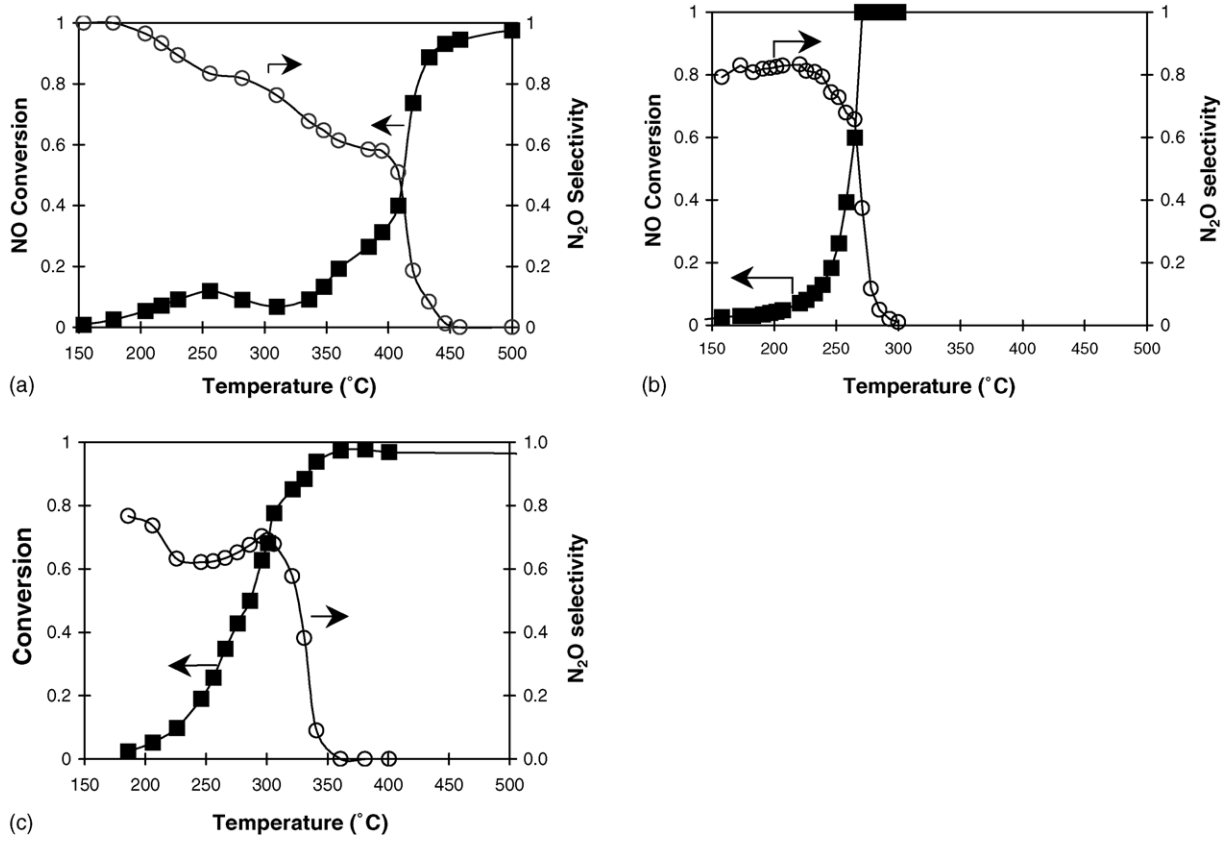

Fig. 12. Comparison of temperature-programmed conversion and selectivity profiles for the CO + NO reaction on Pt/Al_2O_3 (a); Rh/Al_2O_3–CeO_2 (b); Pt–Rh/Al_2O_3 (c) in stoichiometric conditions with 5×10^{-3} atm CO and 5×10^{-3} atm N_2O.

Table 6
Kinetic and thermodynamic data obtained at 300 °C for the CO + NO and CO + N_2O reactions [12,62]

Catalyst	Reaction	P_{CO} (10^{-3} atm)	P_{NO} or P_{N_2O} (10^{-3} atm)	λ_{NO} or λ_{N_2O} (atm^{-1})	λ_{CO} (atm^{-1})	k'_n[a] (atm^{-1}) (10^2 mol h^{-1} at_s^{-1})
Pt/Al_2O_3	CO + NO	5–9	1.5–5.6	11	121	4.0
	CO + N_2O	3.6–13.8	1.8–7.4	90	78	10.0
Rh/Al_2O_3	CO + NO	3–13.6	0.5–3.2	472	71	123.1
	CO + N_2O	3.6–13.8	1.8–7.4	36	50	34.0
$Pt–Rh/Al_2O_3$	CO + NO	3–8	1.5–5.6	505	122	2.8
	CO + N_2O	3.8–10.4	1.5–5.6	66	91	4.2

[a] Intrinsic rate constant for the dissociation step of N_2O (N_2O_{ads} + *→ N_2 + O_{ads} + *) and of NO (NO_{ads} + *→ N_{ads} + O_{ads}) in the mechanism of the CO + N_2O and CO + NO reactions.

reaction. Consequently, the CO + N_2O sub-reaction takes place when NO depletes the surface near 100% NO conversion on Rh/Al_2O_3. The thermal sintering also sharply altered the selectivity behavior of $Pt–Rh/Al_2O_3$ due to a weakening of N_2O adsorption [66].

Now, regarding the weak effect of ceria on the selectivity behavior of $Pt–Rh/Al_2O_3–CeO_2$, the comparison of the relative constant k_{22}/k_{23} for the CO + NO reaction and k_{22}/k_{28} for the single CO + N_2O reaction is relevant. In this latter case, ceria benefits the activity at 300 °C, near the light-off temperature, while in the presence of NO the extensive reduction of ceria suppresses this beneficial effect. Consequently, the subsequent CO + N_2O reaction in the course of the CO + NO reaction on $Pt–Rh/Al_2O_3–CeO_2$ would be catalysed only by noble metals that could explain the weak effect of ceria on the selectivity toward the production of nitrogen.

6. Conclusion

This paper compares kinetic and spectroscopic features of the CO + NO and CO + N_2O reaction mainly on supported Pt- and Rh-based catalysts in order to explain changes in the selectivity behavior toward the production of N_2O, particularly after ceria addition. Basically, in situ spectroscopic observations can be profitably used for discriminating intermediates that could be involved in the CO + NO reaction, particularly on Rh, and for checking the validity of mechanism proposals from steady-state kinetic studies. In addition, spectroscopic observations provide useful information for establishing a rate equation usually based on various assumptions that can be a posteriori validated from these observations. Both comparisons show that kinetic models established for predicting the catalytic performances correctly explain the behavior of noble metals promoted by ceria during the CO + NO reaction in terms of activity and selectivity.

Acknowledgements

We greatly thank the Région Nord-Pas-de-Calais, The CNRS, The IFP, The ADEME for their financial support.

References

[1] K.C. Taylor, Catal. Rev. Sci. Eng. 35 (1993) 457.
[2] M. Shelef, G.W. Graham, Catal. Rev. Sci. Eng. 36 (1994) 433.
[3] T.W. Root, L.D. Schmidt, G.B. Fischer, Surf. Sci. 134 (1983) 30.
[4] R.J. Gorte, L.D. Schmidt, J.-L. Gland, Surf. Sci. 109 (1990) 367.
[5] D.T. Wickam, B.A. Banse, B.E. Koel, Surf. Sci. 243 (1991) 83.
[6] D.G. Castner, G.A. Somorjai, Surf. Sci. 83 (1979) 60.
[7] A.A. Tolia, C.T. Williams, C.G. Takoudis, M.J. Weaver, J. Phys. Chem. 99 (1995) 4599.
[8] C.T. Williams, A.A. Tolia, H.Y.H. Chan, C.G. Takoudis, M.J. Weaver, J. Catal. 163 (1996) 63.
[9] B.K. Cho, J. Catal. 148 (1994) 697.
[10] V.P. Zhdanov, J. Catal. 162 (1996) 147.
[11] B.K. Cho, J. Catal. 162 (1996) 149.
[12] P. Granger, P. Malfoy, G. Leclercq, J. Catal. 223 (2004) 142.
[13] P. Granger, J.-F. Lamonier, N. Sergent, A. Aboukais, L. Leclercq, G. Leclercq, Top. Catal. 16–17 (2001) 1.
[14] P. Fornasiero, G. Ranga Rao, J. Kaspar, F. L'Eratio, M. Graziani, J. Catal. 175 (1998) 269.
[15] G. Ranga Rao, P. Fornasiero, R. Di Monte, J. Kaspar, G. Vlaic, G. Balducci, S. Meriani, G. Gubitosa, A. Cremona, M. Graziani, J. Catal. 162 (1996) 1.
[16] D. Kondarides, T. Chafik, X. Verykios, J. Catal. 193 (2000) 303.
[17] R. Burch, M.D. Coleman, J. Catal. 208 (2002) 435.
[18] T. Chafik, D.I. Kondarides, X.E. Verykios, J. Catal. 190 (2000) 446.
[19] H. Topsoe, J. Catal. 216 (2003) 155.
[20] K.A. Almusaiteer, S.S.C. Chuang, S.D. Tan, J. Catal. 189 (2000) 247.
[21] J. Liang, H.P. Wang, L.D. Spicer, J. Phys. Chem. 99 (1985) 5840.
[22] R. Krishnamurthy, S.S.C. Chuang, M. Balakos, J. Catal. 157 (1995) 512.
[23] B.K. Cho, B.H. Shanks, J.E. Bailey, J. Catal. 115 (1989) 486.
[24] C. Dujardin, A.-S. Mamede, E. Payen, B. Sombret, J.-P. Huvenne, P. Granger, Top. Catal. 30–31 (2004) 347.
[25] P. Granger, H. Praliaud, J. Billy, L. Leclercq, G. Leclercq, Surf. Interface Anal. 34 (2002) 92–96.
[26] R. Dictor, J. Catal. 109 (1988) 89.
[27] A.-S. Mamede, G. Leclercq, E. Payen, J. Grimblot, P. Granger, Phys. Chem. Chem. Phys. 5 (2003) 4402.
[28] A.-S. Mamede, G. Leclercq, E. Payen, P. Granger, J. Grimblot, J. Mol. Struct. 651–653 (2003) 353.
[29] K. Otto, C.P. Hubard, W.H. Weber, G.W. Graham, Appl. Catal. B 1 (1992) 317.
[30] W.H. Weber, R.J. Baird, G.W. Graham, J. Raman Spectrosc. 37 (1988) 239.
[31] B.K. Cho, B.H. Shank, J.E. Bailey, J. Catal. 115 (1989) 486.
[32] A.T. Bell, D. Lorimer, J. Catal. 59 (1979) 223.
[33] R.L. Klein, S.B. Schwartz, L.D. Schmidt, J. Phys. Chem. 89 (1985) 4908.

[34] A. Kudo, M. Steinberg, A.J. Bard, A. Campion, M.A. Fox, T.E. Mallouk, S.E. Weber, J.M. White, J. Catal. 84 (1983) 200.
[35] W.C. Hecker, A.T. Bell, J. Catal. 84 (1983) 200.
[36] P. Granger, C. Dathy, J.J. Lecomte, L. Leclercq, M. Prigent, G. Mabilon, G. Leclercq, J. Catal. 173 (1998) 304.
[37] D. Lorimer, A.T. Bell, J. Catal. 59 (1979) 223.
[38] T.R. Ward, R. Hoffman, M. Shelef, Surf. Sci. 289 (1993) 85.
[39] P. Granger, J.J. Lecomte, C. Dathy, L. Leclercq, G. Leclercq, J. Catal. 175 (1998) 194–203.
[40] K. Almusaiteer, S.C.C. Chuang, J. Catal. 184 (1999) 189.
[41] D.N. Belton, S.J. Schmieg, J. Catal. 144 (1993) 9.
[42] S.K. Ng, D.N. Belton, S.J. Schmieg, G.B. Fisher, J. Catal. 146 (1994) 394.
[43] R.F. Van Slooten, B.E. Nieuwenhuys, J. Catal. 44 (1990) 429.
[44] P. Granger, J.J. Lecomte, L. Leclercq, G. Leclercq, Appl. Catal. A: Gen. 208 (2001) 369.
[45] S.H. Oh, G.B. Fisher, J.E. Carpenter, D.W. Goodman, J. Catal. 100 (1986) 360.
[46] J. Kaspar, C. Leitenburg, P. Fornasiero, A. Trovarelli, M. Graziani, J. Catal. 146 (1994) 136.
[47] C.H.F. Peden, D.N. Belton, S.J. Schmieg, J. Catal. 155 (1995) 204.
[48] S. Kim, M.J. D'Aniello Jr., Appl. Catal. 56 (1989) 23.
[49] P. Granger, L. Delannoy, L. Leclercq, G. Leclercq, J. Catal. 177 (1998) 147.
[50] P. Granger, J.F. Lamonier, N. Sergent, A. Aboukais, L. Leclercq, G. Leclercq, Top. Catal. 16–17 (1–4) (2001) 89.
[51] P. Granger, L. Delannoy, J.J. Lecomte, C. Dathy, L. Leclercq, G. Leclercq, J. Catal. 207 (2002) 202.
[52] A. Aboukais, P. Granger, J.F. Lamonier, J.J. Lecomte, L. Leclercq, G. Leclercq, Colloids Surf. A: Physicochem. Eng. Aspects 158 (1999) 241–247.
[53] S.H. Oh, J. Catal. 124 (2002) 477.
[54] R.H. Nibbelke, M.A. Campman, J.H.B.J.G. Marin, J. Catal. 171 (1997) 358.
[55] J.H. Holles, M.A. Switzer, R.J. Davis, J. Catal. 190 (2000) 247.
[56] L.D. Schmidt, D. Hansenberg, S. Schwartz, G.A. Papapolymerou, in: M.L., Deviney, J.L., Gland, (Eds.), Catalyst Characterisation Science-Surface and Solid State Chemistry, Proceedings of the ACS Symposium Series, vol. 288, Am. Chem. Soc., Washington, DC, 1985, p. 177.
[57] C.G. Takoudis, L.D. Schmidt, J. Catal. 80 (1983) 274.
[58] R.W. Mac Cabe, C. Wong, J. Catal. 121 (1990) 422.
[59] B.K. Cho, B.H. Shanks, J.E. Bailey, J. Catal. 115 (1989) 486.
[60] B.K. Cho, J. Catal. 138 (1992) 255.
[61] B.K. Cho, J. Catal. 148 (1994) 697.
[62] P. Granger, P. Malfoy, P. Esteves, L. Leclercq, G. Leclercq, J. Catal. 187 (1999) 321.
[63] Y. Li, M. Bowker, Surf. Sci. 348 (1996) 181.
[64] V.P. Zhdanov, J. Catal. 162 (1996) 47.
[65] A.A. Diamantis, G.J. Sparrow, J. Colloid Interface Sci. 47 (1974) 455.
[66] P. Granger, F. Dhainant, G. Leclercq, Focus Catal. Res., in press.